JOURNAL OF COMPUTATIONAL PHYSICS 65, 410–431 (1986)

Scattering of a Pulse by a Cavity in an Elastic Half-Space

C. L. SCANDRETT AND G. A. KRIEGSMANN

Department of Engineering Sciences and Applied Mathematics, Technological Institute, Northwestern University, Evanston, Illinois 60201

AND

J. D. ACHENBACH

Department of Civil Engineering and Department of Engineering Sciences and Applied Mathematics, Technological Institute, Northwestern University, Evanston, Illinois 60201

Received March 29, 1985; revised September 3, 1985

The finite difference technique is employed to study plane strain scattering of pulses from finite anomalies embedded in an isotropic, homogeneous, elastic half-space. In particular, the scatterer is taken to by a cylindrical cavity. A new transmission boundary condition is developed which transmits energy conveyed by Rayleigh surface waves. This condition is successfully employed in reducing the domain of numerical calculations from a semi-infinite to a finite region. A test of the numerical scheme is given by considering a time harmonic pulse of infinite extent. The numerical technique is marched out in time until transients have radiated away and a steady state solution has been reached which is found to be in good agreement with results produced by a series type solution. Time domain solutions are given in terms of time histories of displacements at the half-space free surface; and by sequences of snapshots, taken of the entire numerical domain, which illustrate the scattering dynamics.

1. INTRODUCTION

Scattering of a wave pulse by an inhomogeneity in a homogeneous elastic half-space is of interest in several branches of applied science. Examples include exploration seismology, earthquake damage prediction, defect characterization in nondestructive testing, and verification considerations in underground nuclear testing.

Analytical techniques for scattering by a cavity in a half-space have been employed by Ben-Menahem and Cisternas [1], Thiruvenkatachar and Viswanathan [2], and Gregory [3], for solutions in the frequency domain. Each

0021-9991/86 $3.00

used series solutions whose convergence was guaranteed, since the incident wavelength was large relative to a characteristic length of the scatterer. Datta and El-Akily [4] later used the method of matched asymptotics to find the leading order effects generated by a cylindrical cavity subject to time harmonic forcing, under the same assumptions. Use of ray theory and geometrical optics by Achenbach, Gautesen, and McMaken [5] has produced results in the regime of short incident wavelengths for point and line sources in an elastic half-space.

Numerical and analytical techniques have been combined in the work of Datta and Shah [6] who used finite element methods combined with the multipole series approach of Gregory. Dravinski [7], Achenbach *et al.* [8, 9], and Niwa, Kitahara, and Ideka [10] employed boundary integral formulations requiring the use of the complicated Green's function for the elastic half-space.

The scattering of compact pulses by an inclusion in an elastic half-space can, in principle, be described by a superposition of time harmonic solutions. However, since a time harmonic problem must be solved for several frequencies which make up the incident pulse, this Fourier construction is very costly and inefficient. An alternative method is the direct numerical integration of the time dependent equations of motion by either the finite difference or finite element method.

Implementation of direct numerical integration requires, however, the introduction of an artificial boundary to restrict the computations to a finite domain. This is done at the expense of special handling of the solution at this boundary. To properly model conditions at infinity, a condition must be imposed which allows transmission of radiated energy with little or no reflection.

Several papers have considered time dependent finite difference or finite element methods for pulse scattering problems in elastic solids, with a variety of methods to handle the transmission condition applied at an artificial boundary. Early studies [11, 12, 13] allowed energy to be reflected back into the numerical domain with the result that the iteration scheme no longer gave accurate results when spurious reflections contaminated displacement histories of points under consideration. Smith [14] proposed combining solutions produced by applying Neumann and Dirichlet type boundary conditions at surfaces of the artificial boundary. An application of this method is found in Crichlow's [15] study of anti-plane strain scattering from anomalies embedded in a half-space. In principle this scheme completely eliminates reflections, but it is highly inefficient since it requires the solution of at least six Cauchy problems for a given scattering problem. A more efficient approach is provided by local boundary operator methods, since these can be directly incorporated into finite difference schemes with little increase in computational effort. Two examples of local boundary operators are viscous damping applied at the artificial boundary introduced by Lysmer and Kuhlemeyer [16], and the assumption of paraxial propagation based on the operator-splitting techniques of Engquist and Majda [17]. These two techniques are local in that they involve only displacements at or near the artificial boundary. A review of these techniques and their relative effectiveness is given in [18].

Scattering from a finite obstacle embedded in an elastic half-space produces sur-

face waves which propagate energy along the free surface of the half-space. Smith's method effectively cancels reflected Rayleigh waves, but at the expense of producing concommitant body wave reflections which may or may not cancel. Fuyuki and Matsumoto [19] applied transmission conditions developed by Clayton and Engquist [20] (paraxial approximation) at the artificial boundaries of their numerical domain in an attempt to study reflections and transmissions of Rayleigh surface waves striking a trench. They note that upon complete penetration of their artificial boundary by a rayleigh surface wave, instabilities occur which grow in time.

Recently, Scandrett, Kriegsmann, and Achenbach [21] have developed a transmission condition based upon the cylindrical nature of displacements scattered from finite obstacles. It is derived on the basis of asymptotic considerations as the distance from scatterer to artificial boundary (R_b) becomes large. It is equivalent to the second-order boundary operator developed by Engquist and Majda who used the more formidable theory of pseudo-differential operators. In the present study, this operator is extended to allow the transmission of Rayleigh surface waves out of the numerical domain.

The viability of this boundary operator and the associated finite difference scheme is demonstrated here by considering the scattering of a plane compressional pulse by a circular void embedded in a half-space. Solutions are given in terms of time histories of the displacements at the half-space free surface. Sequences of "snapshots" are presented which illustrate the dynamics of the scattering process.

To test the accuracy of the method a time harmonic wave was used in place of the incident pulse to excite the cavity. After transients were allowed to radiate off to infinity, a time harmonic steady state solution evolved that was found to be in excellent agreement with results produced by a multipole series expansion.

Section 2 contains the statement of the scattering problem while Section 3 describes the radiation boundary condition. The numerical scheme is presented in Section 4, and the results for the pulse problem are described in Section 5. Results for a cylindrical cavity in an infinite elastic space are given for comparison and contrast. Finally, the time harmonic results are described and compared to the results of Shah, Wong, and Datta [22].

2. Formulation

Two-dimensional scattering of an incident pulse by a circular cylindrical cavity in a homogeneous isotropic elastic half-space is considered. The elastic solid is characterized by the Lamé constants λ and μ, and the mass density ρ. The incident plane displacement pulse is taken in the form

$$\mathbf{u}' = a\tau^{1/2}\hat{\mathbf{d}}\left[t' - \frac{\mathbf{x}'\cdot\hat{\mathbf{d}}}{c_L}\right] e^{-\tau[t' - \mathbf{x}'\cdot\hat{\mathbf{d}}/c_L]^2} \tag{2.1}$$

where $\hat{\mathbf{d}} = (\cos\theta_I, \sin\theta_I, 0)$, a is the radius of the cavity, $c_L = [(\lambda + 2\mu)/\rho]^{1/2}$ is the

longitudinal wave speed, t' is time, θ_I is the angle which the propagation direction vector $\hat{\mathbf{d}}$ makes with the positive x' axis, and τ, which is of dimension (1/time^2), is a measure of the time interval between peaks of the incident pulse. The pulse given in (2.1) is similar in form to the one used by Alford, Kelly, and Boore [23]. For $\theta_I = 0$, the time variation of the x coordinate of the displacement at $x' = 0$, is sketched in Fig. 1.

Dimensionless quantities t, $\mathbf{x}$, and $\mathbf{u}^I$ are now defined as follows:

$$t = t'\tau^{1/2}, \qquad \mathbf{x} = \mathbf{x}'/a, \qquad \mathbf{u}^I = \mathbf{u}'/a. \tag{2.2}$$

The incident pulse is written in terms of these quantities as

$$\mathbf{u}^I = \hat{\mathbf{d}}(t - \alpha \mathbf{x} \cdot \hat{\mathbf{d}})\, e^{-(t - \alpha \mathbf{x} \cdot \hat{\mathbf{d}})^2}, \tag{2.3}$$

where

$$\alpha = a\tau^{1/2}/c_L \tag{2.4}$$

is a dimensionless number characterizing the pulse. The total dimensionless displacement is split into incident, reflected, and scattered portions

$$\mathbf{u}^T = \mathbf{u}^I + \mathbf{u}^R + \mathbf{u}. \tag{2.5}$$

The reflected displacement $\mathbf{u}^R$ is the pulse that would result from the reflection of the incident pulse off the free surface of the half-space, in the absence of the cylindrical cavity. It is given by

$$\begin{aligned} \mathbf{u}^R = {} & A\hat{\mathbf{d}}_1(t - \alpha \mathbf{x} \cdot \hat{\mathbf{d}}_1)\, e^{-(t - \alpha \mathbf{x} \cdot \hat{\mathbf{d}}_1)^2} \\ & + B(\hat{\mathbf{i}}_3 \wedge \hat{\mathbf{d}}_2)(t - \beta \mathbf{x} \cdot \hat{\mathbf{d}}_2)\, e^{-(t - \beta \mathbf{x} \cdot \hat{\mathbf{d}}_2)^2}, \end{aligned} \tag{2.6}$$

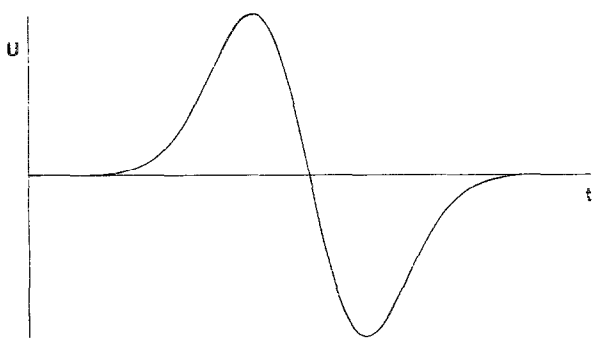

FIG. 1. Indicent longitudinal displacement pulse U versus time: $\Delta = (2/\tau)^{1/2}$ = time interval between pulse peaks.

where $\hat{\mathbf{d}}_1 = (\cos\theta_I, -\sin\theta_I, 0)$, $\hat{\mathbf{d}}_2 = (\cos\theta_T, -\sin\theta_T, 0)$, $\hat{\mathbf{i}}_3 = (0, 0, 1)$, and A and B are the reflection coefficients:

$$A = \frac{\sin 2\theta_T \sin 2\theta_I - (\beta^2/\alpha^2)\cos^2 2\theta_T}{\sin 2\theta_T \sin 2\theta_I + (\beta^2/\alpha^2)\cos^2 \theta_T}, \tag{2.7}$$

$$B = \frac{2(\beta/\alpha)\cos 2\theta_T \sin 2\theta_I}{\sin 2\theta_T \sin 2\theta_I + (\beta^2/\alpha^2)\cos^2 2\theta_T}, \tag{2.8}$$

while

$$\theta_T = \cos^{-1}[(\alpha/\beta)\cos\theta_I], \qquad \beta = a\tau^{1/2}/c_T, \qquad c_T = (\mu/\rho)^{1/2}. \tag{2.9}$$

The scattered field $\mathbf{u}$ is generated by the interaction of the cavity with the incident and reflected fields.

The scattered displacement $\mathbf{u}$ must satisfy

$$\frac{1}{\beta^2}\nabla^2\mathbf{u} + \left(\frac{1}{\alpha^2} - \frac{1}{\beta^2}\right)\nabla\nabla\cdot\mathbf{u} = \ddot{\mathbf{u}}. \tag{2.10}$$

In what follows, two coordinate systems are used to solve the scattering problem. In cylindrical coordinates $\mathbf{u} \equiv (u, v, 0)$, where u and v are the radial and circumferential scattered displacements, respectively. In the rectangular coordinate frame $\mathbf{U} \equiv (U, V, 0)$, where U and V are the scattered displacements in the x and y directions, respectively. The origin of both systems is taken to be the center of the cylindrical cavity while the half-space free surface is the line $y = y_0$ in the rectangular frame. Since the cylindrical cavity is free of surface tractions, the scattered displacements $\mathbf{u}$ must satisfy

$$\frac{1}{\alpha^2}\frac{\partial u}{\partial r} + \left(\frac{1}{\alpha^2} - \frac{2}{\beta^2}\right)\left(u + \frac{\partial v}{\partial\theta}\right) = -\frac{1}{\mu}(\tau^{\mathrm{I}}_{rr} + \tau^{\mathrm{R}}_{rr}) \tag{2.11}$$

$$\frac{\partial v}{\partial r} - v + \frac{\partial u}{\partial\theta} = -\frac{1}{\mu}(\tau^{\mathrm{I}}_{r\theta} + \tau^{\mathrm{R}}_{r\theta}), \tag{2.12}$$

for $r = 1$, $0 \leqslant \theta \leqslant 2\pi$. The stress components τ^{I}_{mn} and τ^{R}_{mn} are surface tractions which result from the presence of the incident and reflected pulses, respectively. At the half-space free surface, $\mathbf{U}$ must satisfy:

$$\left(\frac{1}{\alpha^2} - \frac{2}{\beta^2}\right)\frac{\partial U}{\partial x} + \frac{1}{\alpha^2}\frac{\partial V}{\partial y} = 0 \tag{2.13}$$

$$\frac{\partial U}{\partial y} + \frac{\partial V}{\partial x} = 0, \tag{2.14}$$

at $y = y_0$ and for all x. Figure 2 illustrates the geometry of the problem.

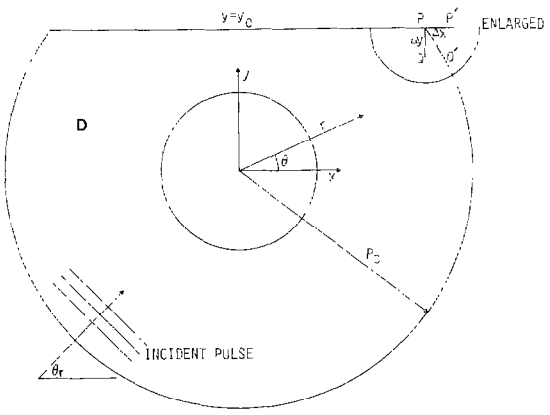

FIG. 2. Geometry of the half-space scattering problem.

As $r \to \infty$, the scattered displacements must behave as outgoing waves. Finally initial conditions must be added to (2.3)–(2.4) to complete the mathematical statement of the problem. Since the system is excited only by the incident pulse, the initial conditions on the scattered displacements are

$$\mathbf{u} \equiv \dot{\mathbf{u}} \equiv \mathbf{U} \equiv \dot{\mathbf{U}} \equiv 0 \qquad \text{for} \quad t = 0,\ |x| < \infty,\ y \leqslant y_0. \tag{2.15}$$

3. Radiation Conditions

In order to solve the problem presented in Section 2 numerically an artificial boundary must be introduced so that the number of iterations in the spatial domain will be finite at any given time level. This artificial boundary must model infinity to the extent that scattered waves are allowed to pass through with little or no reflection. Should reflections from this boundary occur, they would eventually contaminate the desired results elsewhere in the numerical domain. With the addition of free surface of the half-space, radiation conditions at points close to the intersection of the artificial boundary and the free surface will require special attention.

It is well known that when displacements having curved wavefronts impinge on a flat free surface, Rayleigh waves are excited. These surface waves have the properties that: (1) they decay in amplitude with increase of depth into the elastic medium from the free surface and (2) they are nondispersive.

It is expected that Rayleigh waves will be produced from the fields scattered by the cavity, and therefore to ensure outgoing Rayleigh surface waves a special transmission condition must be produced for the artificial boundary in the vicinity of the free surface. Body waves and Rayleigh waves must be allowed to pass out of the numerical domain with little or no reflection.

In [21] transmission boundary conditions have been employed for 2-dimensional problems which appear to be very effective in transmitting transverse and longitudinal waves. These conditions may be represented by

$$A\mathbf{u} = O\left(\frac{1}{R_b^2}\right) \tag{3.1}$$

where

$$A = \begin{pmatrix} \dfrac{\partial}{\partial r} + \dfrac{1}{2r} + \alpha \dfrac{\partial}{\partial t} & \dfrac{\beta - \alpha}{\beta r} \dfrac{\partial}{\partial \theta} \\ \dfrac{\beta - \alpha}{\alpha r} \dfrac{\partial}{\partial \theta} & \dfrac{\partial}{\partial r} + \dfrac{1}{2r} + \beta \dfrac{\partial}{\partial t} \end{pmatrix}. \tag{3.2}$$

This operator is evaluated at R_b, where R_b is the distance from the origin to the artificial boundary of the grid.

Given the material properties of the elastic medium, the Rayleigh wave speed is uniquely determined. Using the scaling provided in Section 2, the Rayleigh surface wave may be written as

$$\mathbf{U}^R = [A_1(y), A_2(y), 0]\, F(\gamma x \pm t), \qquad \gamma = a\tau^{1/2}/c_R \tag{3.3}$$

where U_1^R and U_2^R are horizontal and vertical displacements, respectively. The terms $A_i(y)$ are functions which decay exponentially as $y_0 - y \to \infty$, c_R is the Rayleigh wave speed, and $F(\gamma x \pm t)$ represents a wave form travelling along the free surface of the half-space. The rate at which the amplitudes $A_i(y)$ decay depends on pulse length, with short pulses decaying more rapidly with depth.

The form of the Rayleigh surface waves (3.3) suggests the use of the following radiation condition to allow their passage:

$$B\mathbf{U} = \left(\frac{\partial}{\partial x} \pm \gamma \frac{\partial}{\partial t}\right) \mathbf{U} = 0, \qquad x = \pm x_B \tag{3.4}$$

where $x_B \gg 1$.

The combination of (3.1) and (3.4) will be used in the numerical scheme to ensure proper transmission of waves near the intersection of the free surface and the artificial grid boundary.

As mentioned in Section 2, two coordinate systems are used to solve the half-space scattering problem. Both systems overlap within a region where Rayleigh waves may have a significant amplitude. The radiation condition for body waves (3.1) is given in terms of a cylindrical coordinate system while the radiation condition for Rayleigh waves (3.4) is in terms of a rectangular system. In order to combine these to produce a total radiation condition in either frame, transformation of each radiation condition into the alternative coordinate system must be found. The

transformation from cylindrical coordinate displacements to rectangular coordinate displacements is given by

$$\mathbf{U} = \begin{pmatrix} \cos\theta & -\sin\theta \\ \sin\theta & \cos\theta \end{pmatrix} \mathbf{u}. \tag{3.5}$$

Writing (3.1) in terms of rectangular coordinates we have

$$A\mathbf{u} = \bar{A}\mathbf{U} \tag{3.6}$$

where the elements of $\bar{A}$ are

$$\bar{A}_{11} = \left(1 - \frac{\alpha}{\beta}\sin^2\theta\right)\frac{\partial}{\partial x} + \frac{\alpha}{\beta}\cos\theta\sin\theta\frac{\partial}{\partial y} + \frac{2\alpha-\beta}{2\beta R_b}\cos\theta + \alpha\cos\theta\frac{\partial}{\partial t} \tag{3.7}$$

$$\bar{A}_{12} = \frac{\alpha}{\beta}\cos\theta\sin\theta\frac{\partial}{\partial x} + \left(1 - \frac{\alpha}{\beta}\cos^2\theta\right)\frac{\partial}{\partial y} + \frac{2\alpha-\beta}{2\beta R_b}\sin\theta + \alpha\sin\theta\frac{\partial}{\partial t}. \tag{3.8}$$

The matrix elements $\bar{A}_{22}$ and $\bar{A}_{21}$ can be found from $\bar{A}_{11}$ and $\bar{A}_{12}$ by switching α and β, and reversing the sign of $\bar{A}_{21}$. Therefore, in rectangular co-ordinates the total radiation condition is defined by

$$\bar{A}B\mathbf{U} = O(1/R_b^2). \tag{3.9}$$

Now writing (3.4) in terms of cylindrical coordinates we have

$$\left(\frac{\partial}{\partial x} \pm \gamma\frac{\partial}{\partial t}\right)\mathbf{U} = \bar{B}\mathbf{u}, \tag{3.10}$$

where the elements of $\bar{B}$ are defined as

$$\bar{B}_{11} = \cos^2\theta\frac{\partial}{\partial r} - \frac{\sin\theta\cos\theta}{R_b}\frac{\partial}{\partial\theta} + \frac{\sin^2\theta}{R_b} + \gamma\cos\theta\frac{\partial}{\partial t} \tag{3.11}$$

$$\bar{B}_{12} = -\sin\theta\cos\theta\frac{\partial}{\partial r} + \frac{\sin^2\theta}{R_b}\frac{\partial}{\partial\theta} + \frac{\sin\theta\cos\theta}{R_b} - \gamma\sin\theta\frac{\partial}{\partial t} \tag{3.12}$$

$$\bar{B}_{22} = \bar{B}_{11}, \qquad \bar{B}_{21} = -\bar{B}_{12}. \tag{3.13}$$

The total radiation condition in cylindrical coordinates is therefore

$$A\bar{B}\mathbf{u} = (1/R_b^2). \tag{3.14}$$

The artificial or nonreflecting boundary conditions used in the numerical scheme described in Section 5 are obtained by neglecting the $O(1/R_b^2)$ terms in (3.9) and (3.14) when $r = R_b$.

The truncation error of $O(1/R_b^2)$, upon application of the nonreflecting boundary conditions, is only approximately correct. The combination of the boundary operators (A, $\bar{B}$ in (3.14) and $\bar{A}$, B in (3.9)) is not commutative. In reversing the order of multiplication, additional terms of order $O(h/R_b^2)$ occur where h is the vertical component of the coordinates of the artificial boundary mode where the radiation condition is applied. In the present examples the origin is the center of the cavity so that the most severe truncation error is when $h = y_0$. In view of the above commutativity of the boundary operators is within the degree of accuracy of $O(1/R_b^2)$ provided h is much less than R_b. In practice, terms which have a factor of $O(h/R_b^2)$ in (3.9) and (3.14) are incorporated into the $O(1/R_b^2)$ terms and are neglected.

4. Numerical Scheme

The numerical domain of interest $\mathscr{D}$ is shown in Fig. 2. It is defined as $\mathscr{D} = \{x, y \mid y \leqslant y_0,\ 1 \leqslant (x^2+y^2)^{1/2} \leqslant R_b\}$. For each lattice point of a grid superposed on $\mathscr{D}$, the displacement values are computed and stored for two time levels. Displacements at a succeeding third time level are found explicitly in terms of the immediately preceding two with the aid of a centered difference form of the equations of motion (2.10). Away from free surfaces and from the artificial boundary, Eqs. (2.10) suffice in finding displacements at succeeding time steps. The determination of corresponding displacements at free surfaces and the artificial boundary will be discussed in what follows.

Equation (2.10) is here given in terms of rectangular (U and V) and cylindrical (u and v) frames. In rectangular coordinates the equations are

$$U_{k,l}^{n+1} = -U_{k,l}^{n-1} + a_1 U_{k,l}^{n} + a_2(U_{k+1,l}^{n} + U_{k-1,l}^{n}) + a_3(U_{k,l+1}^{n} + U_{k,l-1}^{n}) + a_4(V_{k+1,l+1}^{n} - V_{k+1,l-1}^{n} + V_{k-1,l-1}^{n} - V_{k-1,l+1}^{n}) \tag{4.1}$$

where

$$a_1 = 2\left[1 - \frac{(\Delta t)^2}{\alpha^2(\Delta x)^2} - \frac{(\Delta t)^2}{\beta^2(\Delta y)^2}\right], \qquad a_2 = \frac{(\Delta t)^2}{\alpha^2(\Delta x)^2}$$

$$a_3 = \frac{(\Delta t)^2}{\beta^2(\Delta y)^2}, \qquad a_4 = \frac{(\Delta t)^2}{4\,\Delta x\,\Delta y}\left(\frac{1}{\alpha^2} - \frac{1}{\beta^2}\right) \tag{4.2}$$

and

$$x = -(R_b^2 - y_0^2)^{1/2} + (k-1)\,\Delta x, \qquad y = y_0 + (l-4)\,\Delta y,\ t = n\,\Delta t. \tag{4.3}$$

The equivalent expression for $V_{k,l}^{n+1}$ can be found by exchanging U and V in (4.1), α and β in (4.2), and reversing the sign of a_4. In Eqs. (4.3) and (4.6), subscripts on the displacements **u** and **U** identify a particular lattice point in the numerical grid, while the superscript n fixes the time level of the displacement.

In cylindrical coordinates the corresponding equations are

$$u_{i,j}^{n+1} = -u_{i,j}^{n-1} + b_1 u_{i,j}^n + b_2 u_{i+1,j}^n + b_3 u_{i-1,j}^n + b_4(u_{i,j+1}^n + u_{i,j-1}^n) + b_5(v_{i,j+1}^n - v_{i,j-1}^n) + b_6(v_{i+1,j+1}^n - v_{i+1,j-1}^n + v_{i-1,j-1}^n - v_{i-1,j+1}^n) \tag{4.4}$$

where

$$b_1 = 2\left[1 - \frac{(\Delta t)^2}{\alpha^2(\Delta r)^2} - \frac{(\Delta t)^2}{\beta^2 r^2}(\Delta\theta)^2 - \frac{(\Delta t)^2}{\alpha^2 r^2}\right], \qquad b_2 = \frac{(\Delta t)^2}{\alpha^2\,\Delta r}[1/\Delta r + 1/2r]$$

$$b_3 = \frac{(\Delta t)^2}{\alpha^2\,\Delta r}[1/\Delta r - 1/2r], \qquad b_4 = \frac{(\Delta t)^2}{\beta^2 r^2(\Delta\theta)^2}$$

$$b_5 = -\frac{(\Delta t)^2}{2r^2\,\Delta\theta}\left(\frac{1}{\alpha^2} + \frac{1}{\beta^2}\right), \qquad b_6 = \frac{(\Delta t)^2}{4r\,\Delta r\,\Delta\theta}\left(\frac{1}{\alpha^2} - \frac{1}{\beta^2}\right) \tag{4.5}$$

$$r = 1 + (i-1)\,\Delta r, \qquad \theta = j\,\Delta\theta. \tag{4.6}$$

The expression for $v_{i,j}^{n+1}$ is given by Eq. (4.4) with the u's and v's exchanged and with the constants (4.5) altered by exchanging α and β while reversing the signs of b_5 and b_6.

At the two free surfaces of the numerical domain the traction free boundary conditions (2.11)–(2.12) and (2.13)–(2.14) must be applied. The conditions are used in such a way as to eliminate the need for the introduction of additional grid points exterior to $\mathscr{D}$. The difference formulation of these conditions is that proposed by Ilan and Lowenthal [24], where the equations of motion and the traction free boundary conditions are incorporated into Taylor series expansions of the displacements at the free surfaces. For the free surface of the half space (rectangular coordinates) the differenced boundary conditions are

$$U_{k,4}^{n+1} = -U_{k,4}^{n-1} + c_1 U_{k,4}^n + c_2 U_{k,3}^n + c_3(U_{k+1,4}^n + U_{k-1,4}^n) + c_4(V_{k+1,4}^n - V_{k-1,4}^n) + c_5(V_{k+1,3}^n - V_{k-1,3}^n) \tag{4.7}$$

where

$$c_1 = 2\left[1 - \frac{(\Delta t)^2}{\beta^2(\Delta y)^2} - \frac{(\Delta t)^2}{\alpha^2(\Delta x)^2}\right], \qquad c_2 = 2\frac{(\Delta t)^2}{\beta^2(\Delta y)^2}, \qquad c_3 = \frac{(\Delta t)^2}{\alpha^2(\Delta x)^2}$$

$$c_4 = \frac{(\Delta t)^2}{2\,\Delta x\,\Delta y}\left(\frac{1}{\alpha^2} - \frac{3}{\beta^2}\right), \qquad c_5 = \frac{(\Delta t)^2}{2\,\Delta x\,\Delta y}\left(\frac{1}{\beta^2} - \frac{1}{\alpha^2}\right). \tag{4.8}$$

The corresponding expressions for $V_{k,4}^{n+1}$ are found by exchanging the U's and V's in (4.7) and the α's and β's in (4.8) (except for c_4), and by changing the signs of c_4 and c_5. At the cylindrical free surface the differenced boundary conditions are

$$\begin{aligned} u_{1,j}^{n+1} = &-u_{1,j}^{n-1} + d_1 u_{1,j}^n + d_2 u_{2,j}^n + d_3(u_{1,j+1}^n + u_{1,j-1}^n) \\ &+ d_4(v_{1,j+1}^n - v_{1,j-1}^n) + d_5(v_{2,j+1}^n - v_{2,j-1}^n) \\ &+ d_6 \left\{ \frac{1}{\mu}(\tau_{rr}^{\mathrm{I}} + \tau_{rr}^{\mathrm{R}}) \Big|_{r=1} \right\}, \end{aligned} \tag{4.9}$$

where

$$\begin{aligned} d_1 &= 2 + \frac{(\Delta t)^2}{\alpha^2}\left[-1 - \frac{2}{(\Delta r)^2} + \left(1 - 4\frac{\alpha^2}{\beta^2}\right)\Big/ \Delta r \right] - \frac{2(\Delta t)^2}{\beta^2(\Delta\theta)^2} \\ d_2 &= \frac{(\Delta t)^2}{\alpha^2\,\Delta r}\left(1 + \frac{2}{\Delta r}\right), \qquad d_3 = \frac{(\Delta t)^2}{\beta^2(\Delta\theta)^2} \\ d_4 &= \frac{(\Delta t)^2}{2\alpha^2\,\Delta\theta}\left[-1 + \left(1 - 4\frac{\alpha^2}{\beta^2}\right)\Big/ \Delta r \right] + \frac{(\Delta t)^2}{2\beta^2\,\Delta\theta}(-1 + 1/\Delta r) \\ d_5 &= \frac{(\Delta t)^2}{2\,\Delta r\,\Delta\theta}\left(\frac{1}{\alpha^2} - \frac{1}{\beta^2}\right), \qquad d_6 = \frac{2(\Delta t)^2}{\beta^2\,\Delta r}. \end{aligned} \tag{4.10}$$

The terms τ_{rr}^{I} and τ_{rr}^{R} are the tractions resulting from the displacements $\mathbf{u}^{\mathrm{I}}$ and $\mathbf{u}^{\mathrm{R}}$, respectively (see Sect. 2). The $v_{1,j}^{n+1}$ may be found by exchanging the u's and v's and by changing $\tau_{rr}^{\mathrm{I}} + \tau_{rr}^{\mathrm{R}}$ to $\tau_{r\theta}^{\mathrm{I}} + r_{r\theta}^{\mathrm{R}}$ in (4.9). In addition, in (4.10) the α's and β's should be exchanged (except in d_6), the term $(1 - 4\alpha^2/\beta^2)/\Delta r$ should be replaced by $-3/\Delta r$, and the signs of d_4, d_5, and d_6 should be reversed.

The artificial boundary is split into three segments. The first segment contains boundary points which are far from the surface of the half-space so that only outgoing body waves (L, T) need be considered. For these points the condition (3.1) is center differenced and combined with the center differenced form of (2.10) (the cross derivative term is backward differenced in the radial coordinate) to yield the following equations for $u_{m,j}^{n+1}$ and $v_{m,j}^{n+1}$:

$$\begin{aligned} u_{m,j}^{n+1} = &\, e_1 u_{m,j}^{n-1} + e_2 u_{m-1,j}^n + e_3 u_{m,j}^n + e_4(u_{m,j+1}^n + u_{m,j-1}^n) \\ &+ e_5(v_{m,j+1}^n - v_{m,j-1}^n) + e_6(v_{m-1,j+1}^n - v_{m-1,j-1}^n) \end{aligned} \tag{4.11}$$

where

$$q = \left\{ \Delta t\left(1 + \frac{\Delta r}{2R_b}\right) + \alpha\,\Delta r \right\}^{-1} \tag{4.12}$$

$$e_1 = q\left\{ \Delta t\left(1 + \frac{\Delta r}{2R_b}\right) - \alpha\,\Delta r \right\}, \qquad e_2 = 2q(\Delta t)^2/\alpha\,\Delta r,$$

$$e_3 = -e_2 - 2e_4 + q\left\{-\frac{(\Delta t)^2}{\alpha R_b}\left(1+\frac{3\,\Delta r}{2R_b}\right)+2\alpha\,\Delta r\right\}$$

$$e_4 = \alpha(\Delta t)^2\,\Delta r q/\beta^2 R_b^2(\Delta\theta)^2$$

$$e_5 = \frac{\beta\,\Delta r(\Delta t)^2 q}{2R_b\,\Delta\theta}\left\{\left(\frac{1}{\Delta r}+\frac{1}{R_b}\right)\left(\frac{1}{\alpha}-\frac{1}{\beta}\right)^2+\frac{1}{\alpha\beta R_b}\left(1+\frac{\beta}{\alpha}\right)\right\}$$

$$e_6 = \frac{\alpha(\Delta t)^2 q}{2R_b\,\Delta\theta}\left(\frac{1}{\beta^2}-\frac{1}{\alpha^2}\right). \tag{4.13}$$

The subscript m corresponds to the points where $r \equiv R_b$ (see Eq. 4.6). To find the equation for $v_{m,j}^{n+1}$ exchange the u's and v's in (4.11), α's and β's in (4.13), and reverse the signs of e_5 and e_6.

The second segment of the artificial boundary includes points where the Rayleigh wave displacements, which decay exponentially with distance from the free surface, are not negligible. The condition on this segment is taken from a differenced form of equation (3.14). The following notation is introduced:

$$D_0^x U_{k,l}^n = \frac{1}{2\,\Delta x}(U_{k+1,l}^n - U_{k-1,l}^n), \qquad D_-^x U_{k,l}^n = \frac{1}{\Delta x}(U_{k,l}^n - U_{k-1,l}^n)$$

$$D_+^x U_{k,l}^n = \frac{1}{\Delta x}(U_{k+1,l}^n - U_{k,l}^n), \qquad D_0^{xx} U_{k,l}^n = \frac{1}{(\Delta x)^2}(U_{k+1,l}^n - 2U_{k,l}^n + U_{k-1,l}^n). \tag{4.14}$$

Equation (3.14) is differenced as follows:

$$\{f_1 D_0^{rr} + f_2 D_0^r + f_3 D_0^t D_-^r + f_4 D_0^{tt} + f_5 D_0^t\}\, u_{m,j}^n + \{f_6 D_0^{rr} + f_7 D_0^\theta D_-^r + f_8 D_0^t D_-^r + f_9 D_0^\theta D_-^t + f_{10} D_0^{tt}\}\, v_{m,j}^n = 0 \tag{4.15}$$

where

$$f_1 = \cos^2\theta, \quad f_2 = \frac{\cos^2\theta}{2R_b} + \frac{\beta-\alpha}{\beta R_b}\cos^2\theta, \quad f_3 = \gamma\cos\theta + \alpha\cos^2\theta, \quad f_4 = \gamma\alpha\cos\theta$$

$$f_5 = \frac{\gamma}{2R_b}\cos\theta + \gamma\left(\frac{\beta-\alpha}{\beta R_b}\right)\cos\theta, \qquad f_6 = -\sin\theta\cos\theta, \qquad f_7 = \frac{\beta-\alpha}{\beta R_b}\cos^2\theta$$

$$f_8 = -\gamma\sin\theta - \alpha\cos\theta\sin\theta, \qquad f_9 = \gamma\left(\frac{\beta-\alpha}{\beta R_b}\right)\cos\theta, \qquad f_{10} = -\gamma\alpha\sin\theta. \tag{4.16}$$

A second equation is produced by switching $u_{m,j}^n$ and $v_{m,j}^n$ in (4.15), and by exchanging α and β while reversing the signs of f_6, f_7, f_8, f_9, and f_{10} in (4.16). The two equations have four unknowns $u_{m,j}^{n+1}$, $v_{m,j}^{n+1}$, $u_{m+1,j}^n$, and $v_{m+1,j}^n$. The equations of motion (4.4) with $i = m$ are used to solve for $u_{m+1,j}^n$ and $v_{m+1,j}^n$ in terms of $u_{m,j}^{n+1}$ and

$v_{m,j}^{n+1}$. These values are substituted into Eqs. (4.15) resulting in a 2×2 matrix problem whose solution provides the values $u_{m,j}^{n+1}$ and $v_{m,j}^{n+1}$. The boundary operator (4.15) has a disadvantage in that the f's are theta dependent. Therefore, at every point where (4.15) is applied, a new set of constants must be found. Fortunately, because of the exponential decay Rayleigh waves, relatively few boundary points in the vicinity of the free surface require this special boundary operator.

The final section of the artificial boundary consists of the two points where the free surface and the artificial boundary intersect. Let U_p, V_p, U_Q, and V_Q represent horizontal and vertical displacements at these points (see Fig. 2). Point P is the intersection while Q is located directly below P at a distance Δy. At P the strategy is taken that both radiation conditions (3.1) and (3.4) are applied as well as the free surface boundary conditions (2.13)–(2.14). At Q, (3.1) and (3.4) are applied in conjunction with the equations of motion (2.10). Using the notation (4.14), (3.9) is written as

$$\{g_1 D_0^{xx} + g_3 D_0^x D_-^y + g_5 D_0^{tt} + g_7 D_0^t D_-^x + g_9 D_0^x D_-^y + g_{11} D_0^x + g_{12} D_0^t\}\, U_p^n + \{g_2 D_0^{xx} + g_4 D_0^x D_-^y + g_6 D_0^{tt} + g_8 D_0^t D_-^x + g_{10} D_0^t D_-^y\}\, V_p^n = 0 \tag{4.17}$$

where

$$g_1 = 1 - \frac{\alpha}{\beta}\sin^2\theta, \qquad g_2 = \frac{\alpha}{\beta}\cos\theta\sin\theta,$$

$$g_3 = \frac{\alpha}{\beta}\cos\theta\sin\theta, \qquad g_4 = 1 - \frac{\alpha}{\beta}\cos^2\theta$$

$$g_5 = \gamma\alpha\cos\theta, \qquad g_6 = \gamma\alpha\sin\theta,$$

$$g_7 = \gamma\left(1 - \frac{\alpha}{\beta}\sin^2\theta\right) + \alpha\cos\theta, \qquad g_8 = \gamma\frac{\alpha}{\beta}\cos\theta\sin\theta + \alpha\sin\theta,$$

$$g_9 = \gamma\frac{\alpha}{\beta}\cos\theta\sin\theta, \qquad g_{10} = \gamma\left(1 - \frac{\alpha}{\beta}\cos^2\theta\right),$$

$$g_{11} = \frac{2\alpha - \beta\cos\theta}{2\beta}\frac{\cos\theta}{R_b}, \qquad g_{12} = \gamma\left(\frac{2\alpha-\beta}{2\beta}\right)\frac{\cos\theta}{R_b}. \tag{4.18}$$

A second equation results by exchanging U_p^n and V_p^n in equation (4.17), while exchanging α and β in (4.18), and by reversing the sign on the g's with even subscripts (except for g_{12}). Equation (4.17) is applied at P where outgoing Rayleigh waves are traveling in the position x direction. Similar equations must be written for the other intersection point of the free surface and the artificial boundary. These equations are found by changing D_-^x to D_+^x in (4.17) and by substituting γ for $-\gamma$ in (4.18). At the point Q Eq. (4.17) is applied changing U_p^n and V_p^n to U_Q^n and V_Q^n, and D_-^y to D_+^y. Similarly for the point at the other end of the free surface, change D_-^x to D_+^x and γ to $-\gamma$, in (4.17) and (4.18), respectively.

Equations (4.17) applied to points P and Q, as specified above, results in four equations with eight unknowns. The unknown values are U_P^{n+1}, U_Q^{n+1}, V_P^{n+1}, V_Q^{n+1}, $U_{P'}^n$, $V_{P'}^n$, $U_{Q'}^n$, and $V_{Q'}^n$, where the pseudonodes P' and Q' are also shown in Fig. 2. They are located Δx beyond the edge of the rectangular domain which ends at points P and Q. The values at the pseudonodes are expressed in terms of U_P^{n+1}, V_P^{n+1}, U_Q^{n+1}, and V_Q^{n+1} by application of equations (4.7) at point P and (4.1) at point Q. Substitution of these expressions into the four equations found by applying (4.17) results in a 4×4 matrix equation whose solution provides the unknown values of U^{n+1} and V^{n+1} at P and Q. A similar process is used to find the displacements at the other intersection point of the free surface and the artificial grid boundary.

In the vicinity of the free surface of the half-space, the rectangular and cylindrical coordinate frames overlap. Due to the explicit nature of the proposed difference scheme, values of the displacements at the $(n+1)$st time level may be found for all points except those at the "edge" of each coordinate frame in the overlap region. The spatial meshes are chosen so that points along these "edges" are completely contained in a subdomain of the opposing coordinate system for which displacements at each lattice point for the $(n+1)$st time level are known. The $(n+1)$st displacement for an "edge" point is found by interpolating displacements from a mesh cell containing the edge point and performing a coordinate translation (3.5) of the displacements to the correct system. This process of interpolation and translation must be done at each time step but can be made efficient by finding the "edge" points, interpolation factors, interpolation cells, and translation factors once, and using their stored values repeatedly.

The stability of the finite difference scheme and the boundary conditions is difficult to assess theoretically. If the boundary conditions are ignored a Von Neuman stability analysis may be performed on the difference Eqs. (4.1)–(4.4). Such an analysis was done by Alterman and Karal [11], and Alterman and Loewenthal [25]. They found that Δt must satisfy

$$\Delta t \leqslant \min\{\Delta r, \Delta\theta, \Delta x, \Delta y\} \Big/ \left(\frac{1}{\alpha^2}+\frac{1}{\beta^2}\right)^{1/2} \tag{4.19}$$

to insure stability.

A full stability analysis applying the theory of Gustafsson, Kreiss, and Sundström [26] would be very difficult for the present problem. It was found by conducting numerical experiments, which will be reported in the next section, that when dispersion was properly minimized, instabilities were avoided in the present applications which involve the discretized transmission and free surface boundary conditions and the discrete versions of the equations of motion (4.1) and (4.4).

Dispersion of finite difference approximations to wave equations has been studied recently by Trefethen [27]. He reported that phase and group velocities resulting from a finite difference solution to the elastodynamic equations of motion differ from the true analytical values by terms that are directionally dependent and which

contain a factor of Q^{-2}, where Q represents the number of mesh points used per wavelength. In order to prevent high frequency noise from eventually contaminating results elsewhere in the numerical domain, Q was held relatively high, and pulses where restricted to having smooth leading and trailing edges.

5. Results

Results for time dependent problems in elastodynamics are typically given in one of two forms. One is to isolate points of interest in the spatial domain and chronicle their displacement histories. A second method uses "snapshots' of the displacement fields at specified times of the scattering process for a portion (or all) of the spatial domain. A series of these snapshots could be made to produce a motion picture of the pulse scattering process. The two forms of representation are complementary in as much as one fixes points in space while the other fixes points in time.

Both methods of representation are used in what follows. Relatively few snapshots are given for each of the pulse problems, however, and their presence is only for purposes of illustration. In viewing the snapshots, one should imagine a series of evenly spaced horizontal and vertical lines which overlay the numerical domain. Any deviation from this uniformity is the result of an incident, reflected, or scattered displacement, or a combination of these.

First considered, is scattering of a pulse by a cavity in an unbounded elastic solid. The relevant parameters are: $\Delta r = 0.1$, $\Delta\theta = \pi/30$, $R_b = 5$, $\alpha = 0.8$, $\beta = 1.6$, and $\Delta t = 0.06$. Results for this problem are presented for comparison with results produced by scattering of a pulse from a cylindrical cavity embedded in a half-space. Figures 3a, b, c, and d show snapshots of the pulse (Eq. 2.3 with $\theta_I = 90°$) interacting with the cavity. In Figs. 3a and b the pulse has almost traverse the cavity while in Figs. 3c and d it has nearly disappeared from the numerical domain. Figure 3d best illustrates the scattered L and TV waves. The L waves are most clearly evident on the illuminated side of the cavity, while scattered TV waves can be seen in the shadow zone. The two types of waves are identified by observing subsequent snapshots and determining the relative rate at which they exit the domain.

Figure 4 chronicles time histories of the total displacement for points on the surface of the cavity, shown schematically directly above the histories. Points A and E are in line with the direction of propagation of the incident pulse, where A is on the illuminated side, and E on the shadow side. Due to symmetry the circumferential displacements at A and E are zero as shown. The time scale for the displacement histories is given by equation (2.2); τ was taken to be one, so a time interval of $\sqrt{2}$ should be expected between response peaks, as is verified by the time history of the radial displacement at point A. In what follows let Δ represent this time interval. Several observations can be made of the pulse at the shadow portion of the cavity as recorded at point E. Since the incident pulse first pulls on and then pushes the cavity, the sign of the displacements at E are opposite to those at A since the direction of increasing radial displacement is reversed. It is observed that the time inter-

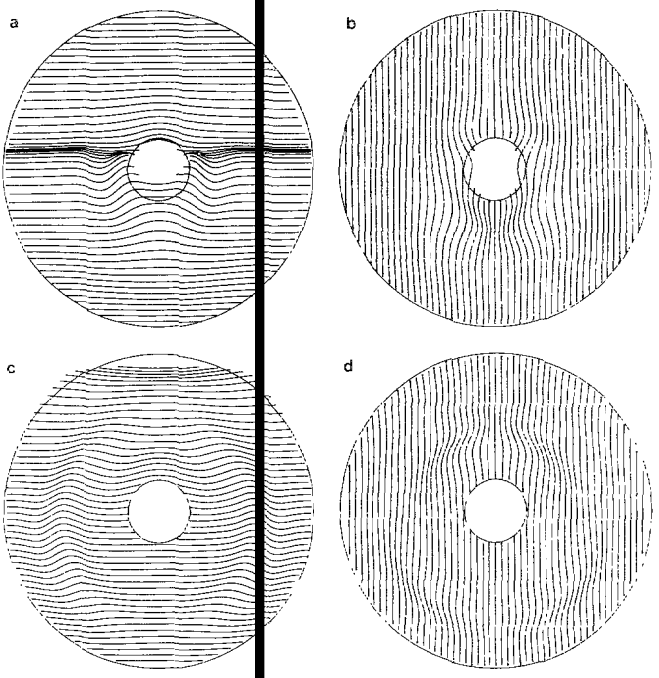

FIG. 3. Snapshots of scattering of a longitudinal displacement pulse from a cylindrical cavity in an elastic space (2D). Figures a and b are vertical and horizontal displacements, respectively, at a time prior to that displayed by c and d. Relevant parameters are: $\Delta r = 0.1$, $\Delta\theta = \pi/30$, $\Delta t = 0.06$, $R_b = 5$, $\alpha = 0.8$, and $\beta = 1.6$.

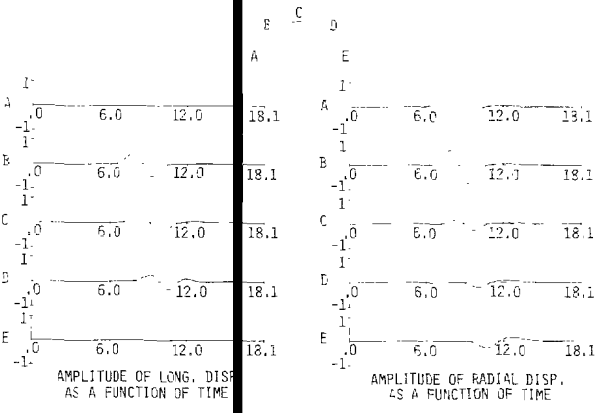

FIG. 4. Time histories of displacements for various points on the cylindrical-cavity free surface (free surface problem). Parameters same as for Fig. 3.

val between peaks (Δ) at E is a factor of about $\sqrt{2}$ greater than that at point A, while the amplitude of the displacement at E relative to that at A is decreased by roughly one-third. In addition, if the cavity were absent the incident pulse would traverse the distance from A to E in 1.6 time units, but in its presence the time between observed peaks at A and E is nearly two times this amount.

Attention is now turned to the problem of scattering of the same pulse as used above from a cylindrical cavity embedded in a half-space whose free surface is normal to the direction of propagation in the incoming wave. The parameters α, β, and Δr are the same as for the free space problem while $\Delta\theta = \pi/64$, $\Delta t = 0.03$, $R_b = 3$, and the new parameters: $y_0 = 1.8$ (depth from free surface to center of cavity), $\Delta x = \Delta y = 0.1$, and $\theta_I = 90°$ (propagation direction of incident pulse). Figures 5a–d are snapshots at times roughly equivalent to those shown in Figs. 3a–d. The values of R_b for the present and preceding problem could have been made equal. In the half space problem a small R_b was chosen for economy of computational effort, while for the full space problem a larger R_b was used because a clear depiction of the scattered displacements was desired.

Because of the relatively small size of R_b for the half-space problem, it is particularly difficult to separate surface and body wave components of the scattered displacements. For larger values of R_b it may be possible to isolate the Rayleigh surface wave but this is not done in the present work.

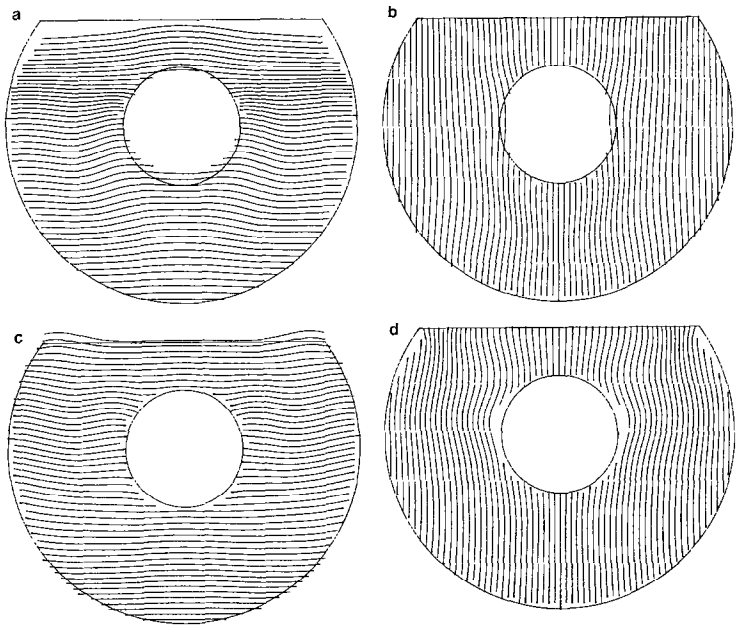

FIG. 5. Snapshots of scattering of a longitudinal pulse (same as used in Fig. 3) from a cylindrical cavity embedded in an elastic half-space. Figures c and d represent a later time than that represented by a and b. Parameters are: $\Delta r = 0.1$, $\Delta\theta = \pi/64$, $\Delta x = \Delta y = 0.1$, $R_b = 3$, $y_0 = 1.8$, $\alpha = 0.8$, $\beta = 1.6$, $\theta_I = 90°$, $\Delta t = 0.03$.

An additional input parameter required for the half-space problem is the depth to which the combined radiation condition (3.14) is applied. In each of the remaining experiments this depth was equal to the depth of the cavity (y_0). Numerical tests to study the effects of varying this depth have not been performed. One would expect, however, that the optimal depth of application should depend upon the shape, duration, and angle of incidence of the incident pulse.

Time histories for this problem (Fig. 6) are given in terms of horizontal and vertical displacements, in contrast to the radial and circumferential displacements of Fig. 4, so care must be taken in comparing equivalent histories. For example, the vertical displacement history at point A of Fig. 6 is to be compared with the radial displacement at point E in Fig. 4 while the vertical displacement at point C in Fig. 6 should be compared with the negative radial displacement history at A in Fig. 4 (since the direction of positive radial displacement at A is downward).

Note that symmetry of the problem demands zero horizontal displacement at points C, A, and G, as observed in Fig. 6. Furthermore, horizontal displacements at points equidistant from this axis are opposite in sign. With information taken from the free space problem, arrival times of positive peaks recorded at point C may be determined and are found to agree well with what is observed. The first peak (at

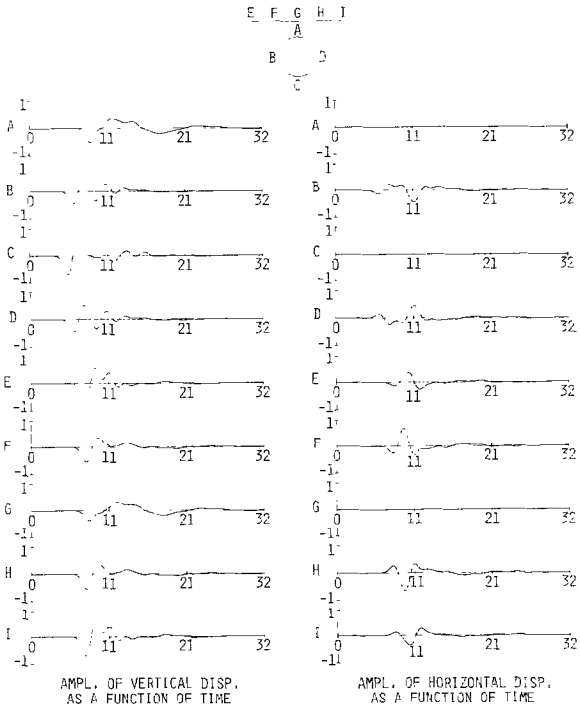

FIG. 6. Time histories of displacements for various points on the cavity and half-space free surfaces. Parameters same as in Fig. 5.

point C) is due directly to the incident pulse, while the second results from a scattered pulse caused by the reflection of the incident wave at the half-space free surface. The third peak appears at a time that a pulse at A (caused by scattering of the incident wave) has been reflected from the free surface of the half-space and has produced a second scattered pulse at point C.

The results suggest that a damped vibration model is excited between the free surfaces of the cavity and the half-space. This can be seen in the slight ringing of the vertical displacements for time histories of points A and G. The relatively long period of this oscillation may be attributed to the elongation of the scattered wave and its multiple reflections as they travel around the cylinder.

Results for a pulse incident under an angle of 45° are shown in Figs. 7–8. All parameters are the same as for the normal incident compressional wave except $\theta_I = 45°$. These results are more difficult to anayze than for the normally incident case because of the appearance of a reflected transverse wave. One observation is that the magnitude of the ringing phenomenon between points A and G has been reduced, as one might expect for incident angles other than normal to the free surface of the half-space.

With the given set of parameters for the half-space scattering problems it was found that each time iteration took approximately one third of a second on a CYBER 170/730.

Several factors should be taken into account when applying the numerical technique presented here to similar pulse scattering problems. The method works most

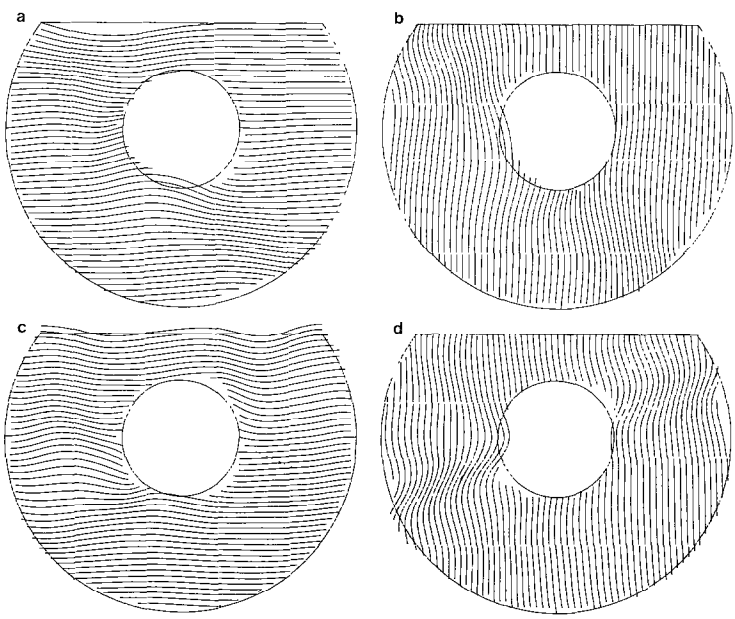

FIG. 7. Same as Fig. 5 except $\theta_I = 45°$.

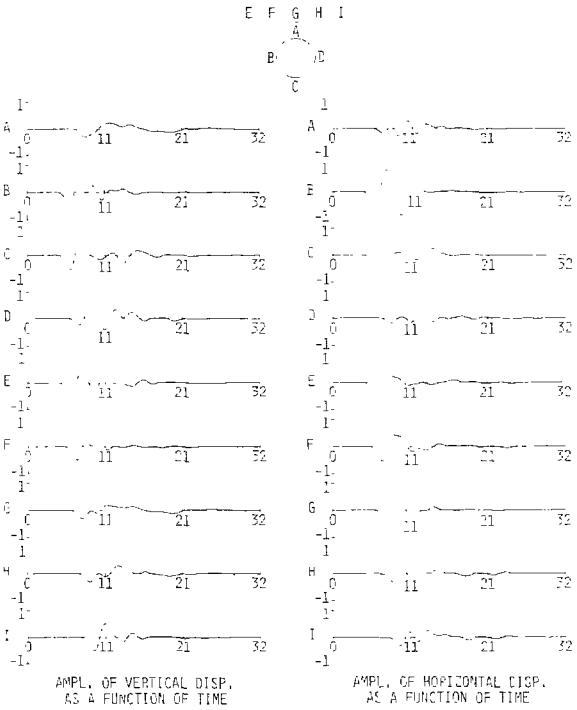

FIG. 8. Time histories of displacements for various points on the cavity and half-space free surfaces. Parameters same as in Fig. 7.

efficiently when the depth of the scatterer and the wavelengths which dominate in the incident pulse are of the same order of magnitude as a characteristic length of the scatterer. If wavelengths dominating the pulse are short (relative to the dimensions of the scatterer) a very fine mesh must be employed in order to minimize grid dispersion. If the depth of the scatterer is relatively large, the corresponding free surface of the half-space and the scatterer can be accounted for, and also to properly apply the radiation boundary operator developed for the numerical scheme.

An argument identical to that presented in [21] (Appendix *A*) can be used to demonstrate the non-existence of bound states for the half-space scattering problem. The absence of such states justifies implementation of the numerical technique presented to solve problems of time harmonic scattering. This is done here to demonstrate the versatility and the accuracy of the method. A multiple series solution (24 terms) provided by Wong is used as a basis of comparison. Shah, Wong, and Datta [22] employed a similar benchmark to test the accuracy of their numerical scheme.

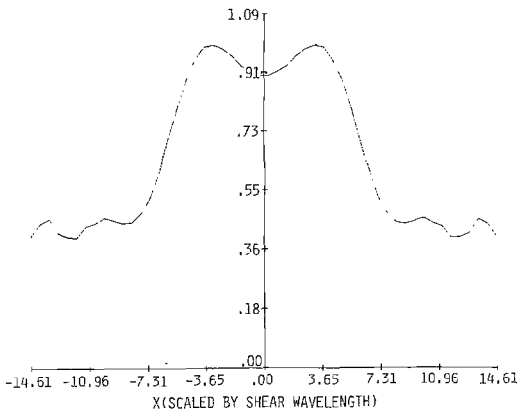

FIG. 9. Magnitude of the scattered vertical displacements at the half-space free surface for an incident time harmonic longitudinal wave. Relevant parameters are: $\Delta r = 1$, $\Delta\theta = \pi/59$, $\Delta x = \Delta y \sim 0.1$, $\Delta t = 0.1$, $R_b = 3$, $y_0 = 1.53$, $\beta = 5.662$, $\alpha = 2.75$, $\theta_I = 90°$.

For the time harmonic problem, the relevant parameters were $\beta = 5.662$, $\nu = 0.3456$ (Poisson's ratio), $\Delta r = \Delta t = 0.1$, $\Delta\theta = \pi/59$, and $\Delta x = \Delta y \sim 0.1$. The numerical scheme was marched forward in time until a steady state solution was reached (measured by the variation of horizontal and vertical displacements at the half-space free surface). Figure 9 displays the comparison of the present numerical technique (solid line) with that of the series solution (dotted line) for the magnitude of the vertical displacement along the half-space. As can be seen, the results compare favorably.

ACKNOWLEDGMENTS

The work of two of the authors (C. L. Scandrett and J. D. Achenbach) was carried out under Contract DE-AC02-83ER13036.A002 with the Department of Energy, Office of Basic Energy Sciences, Engineering Research Program. The work of G. A. Kriegsmann was supported by NSF Grant MCS-8300578.

REFERENCES

1. A. BEN-MENAHEM AND A. CISTERNAS, *J. Math. Phys.* **42**, 112 (1963).
2. V. R. THIRUVENKATACHAR AND K. VISWANATHAN, *J. Math. Mech.* **14**, 541 (1965).
3. R. D. GREGORY, *Proc. Cambridge Philos. Soc.* **67**, 689 (1970).
4. S. K. DATTA AND N. EL-AKILY, *J. Acoust. Soc. Am.* **64**, 1692 (1978).
5. J. D. ACHENBACH, A. K. GAUTESEN, AND H. MCMAKEN, *Ray Methods for Waves in Elastic Solids* (Pitman, Boston, 1982).
6. S. K. DATTA AND A. H. SHAH, *Wave Motion* **4**, 265 (1982).
7. M. DRAVINSKI, *Earth. Eng. St. Dyn.* **11**, 313 (1983).
8. J. D. ACHENBACH AND R. J. BRIND, *J. Sound Vib.* **76**, 43 (1981).

9. J. D. ACHENBACH, W. LIN AND L. M. KEER, *IEEE Trans. Sonics Ultrason.* **SU-30**, 270 (1983).
10. Y. NIWA, M. KITAHARA, AND H. IKEDA, *Theor. Appl. Mech.* **32**, 183 (1984).
11. Z. ALTERMAN AND F. KARAL, *Bull. Seismol. Soc. Amer.* **58**, 367 (1968).
12. D. BOORE, "Finite Difference Methods for Seismic Wave Propagation in Heterogeneous Materials," *Methods in Computational Physics Advances in Research and Applications*, Vol. 11, edited by B. A. Bolt (Academic Press, New York, 1972).
13. A. ILAN, A. UNGAR AND Z. ALTERMAN, *Geophys. J. Roy. Astron. Soc.* **43**, 727 (1975).
14. W. D. SMITH, *J. Comput. Phys.* **15**, 492 (1974).
15. J. M. CRICHLOW, *Geophys. J. Roy. Astron. Soc.* **70**, 563 (1982).
16. J. LYSMER AND R. L. KUHLEMEYER, *J. Eng. Mech. Div. Amer. Soc. Civ. Eng.* **95**, 859 (1969).
17. B. ENGQUIST AND A. MAJDA, *Commun. Pure Appl. Math.* **32**, 313 (1979).
18. E. KAUSEL AND J. L. TASSOULAS, *Bull. Seismol. Soc. Amer.* **71**, 143 (1981).
19. M. FUYUKI AND Y. MATSUMOTO, *Bull. Seismol. Soc. Amer.* **70**, 2051 (1980).
20. R. CLAYTON AND B. ENGQUIST, *Bull. Seismol. Soc. Amer.* **67**, 1529 (1977).
21. C. L. SCANDRETT, G. A. KRIEGSMANN, AND J. D. ACHENBACH, *SIAM J. Sci. Stat. Comput.*, in press.
22. A. H SHAH, K. C. WONG, AND S. K. DATTA, *Wave Motion* **7**, 319 (1984).
23. R. M. ALFORD, K. R. KELLY, AND D. M. BOORE, *Geophysics* **39**, 834 (1974).
24. A. ILAN AND D. LOEWENTHAL, *Geophys. Prospect.* **24**, 431 (1976).
25. Z. ALTERMAN AND D. LOEWENTHAL, *Geophys. J. Roy. Astron. Soc.* **20**, 101 (1970).
26. L. N. TREFETHEN, *J. Comput. Phys.* **49**, 199 (1983).
27. L. N. TREFETHEN, *SIAM Rev.* **24**, 114 (1982).